Kovove Mater. 59 2021 269–278
DOI: 10.4149/km_2021_4_269

Isothermal oxidation kinetics of laser cladded NiCoCrAl/WC + La_2O_3 hybrid composite coatings at 700 ℃

P. Ashtari, N. Parvinai Ahmadi*, S. Yazdani**

Faculty of Materials Engineering, Sahand University of Technology, Tabriz, Iran

Received 30 November 2020, received in revised form 12 June 2021, accepted 11 August 2021

Abstract

NiCoCrAl/WC + (1–4) wt.% La_2O_3 coatings were cladded on H13 tool steel using Nd: YAG pulsed laser. Scanning electron microscopy, wavelength dispersive X-ray spectroscopy, electron probe microanalysis, and X-ray diffraction are used to study the coatings and oxide layers. The oxidation kinetics analysis of coatings at 700 ℃ in a static air atmosphere shows that the oxidation of coatings with La_2O_3 slows down or stops while a compact and stable oxide layer is formed. The formation of $NiCr_2O_4$ spinel makes the oxide layer compact and blocks the connection paths connecting the coating/oxidizing environment. A study of the oxidation mechanism revealed that in coatings with La_2O_3, short-path diffusion has been preferred due to a fine dendritic microstructure and sufficient opportunity to form $NiCr_2O_4$ spinel. Addition of up to 2 wt.% La_2O_3 makes the coatings effectively resist oxidation. An equation has been derived for the oxidation kinetics using the data analyzed with Python™ software.

K e y w o r d s: kinetics of oxidation, laser cladding, composite coating, high temperature, isothermal oxidation

1. Introduction

Nickel-based alloys are used extensively in corrosive environments, which are subjected to wear, relatively high temperature, and fatigue due to their good corrosion and fatigue resistance. However, they do not individually meet the industrial requirements. According to the research, metal-based composites have several applications in increasing the life span of parts such as rollers, piston rods, turbines, etc. The ceramic reinforcement particles such as tungsten, titanium, and vanadium carbides contribute to a good wear resistance from which tungsten carbide (WC) is extensively applied due to suitable wettability with nickel and high hardness (up to 2700 Vickers) [1–7]. The rare-earth metal oxides, such as lanthanides, decrease the surface energy and create the required energy for the nucleation. On the other hand, they adhere to the solid/melt interface and prevent grains growth due to the high atomic radius. So using the oxides of these metals (i.e., La, Ce, Sm, Y, etc.) cause to approach a less defected coating with fine and coaxial dendrites, which not only improve the hardness, fatigue, and corrosion resistance but also result in a decreased stress concentration in the coating/substrate interface and prevent the formation of defects such as crack and porosity in the metal matrix which result in the optimization of coatings thermal properties such as the high-temperature corrosion and thermal shock resistance [7–15].

Currently, methods such as plasma spray, arc welding, laser cladding, and high-velocity oxy-fuel (HVOF) thermal spray are used in metal-based composite coatings production where the laser technique is increasingly being used because of several advantages such as good coating adhesion to the substrate, and defects decrease like porosities, cracks, etc. [1, 16, 17]. The low heat input in this method causes very low coating/substrate mixing (dilution). Consequently, a narrow heat-affected zone (HAZ) creates minimal distortion and contortion [18]. Laser-clad hard composite coatings improve the useful life of industrial parts that are subjected to wear and corrosion, such as dies, cylinders, and rollers [19–21].

*Corresponding author: Parvini@sut.ac.ir
**Corresponding author: Yazdani@sut.ac.ir

Table 1. Chemical composition of NiCoCrAl powder (wt.%)

	Ni	Co	Cr	Al	W
NiCoCrAl	36.164	32.178	19.862	9.291	2.505

AISI H13 steel is a chromium, molybdenum, and vanadium containing hot working tool steel with high hardenability and excellent toughness, which is routinely used for making dies, extrusion mandrels, plastic molds, cores, die holder blocks, and hot work punches. However, for the bulk of hot forming applications like forging and die casting, both wear/erosion and corrosion resistance properties of AISI H13 tool steel at the room as well as elevated temperatures needs to be improved. Several studies have used laser treatment in various methods (e.g., cladding, laser hardening) to extend the longevity of the dies and save in costs for replacements. Various composite coatings have been studied to improve wear and corrosion resistance under high temperatures on various substrates, including steel [22]. On the other hand, very few studies have been performed on metal-based hybrid composites as coatings to extend the longevity of industrial components. Most studies have focused on polymer-based hybrid composites used as biomaterials. Combining this information, we have conducted an experiment to optimize a favorable composition and process to extend the longevity of H13 hot working tool steel.

This paper aims to provide a new hybrid composite coating to extend the life of forging and extrusion dies and provide an option for repairing damaged dies. Laser-coating nickel-based matrix hybrid composite coating onto H13 can provide a cost-effective and more durable option for industries comparable to similar composite coatings.

This paper aims to study the isothermal oxidation of H13 hot work tool steel at 700 ℃, which is laser cladded using nickel powder as the base alloy, 30 wt.% tungsten carbide, and 1–4 wt.% La_2O_3 powders as of first and second reinforcers, respectively.

2. Materials and methods

Nickel-based super-alloy powder (NiCoCrAl) was used as the composite coating matrix with particle size in the range of 45–125 μm. The powder properties are presented in Table 1. 30 wt.% commercial tungsten carbide powder, WC-12Co (Zhuzhou Jiangwu Boda^{TM}) with the particle size in the range 15–45 μm was added as carbide reinforcer to the matrix powder. The mentioned composition was considered a base to maintain the toughness of the coatings and determine more precisely the La_2O_3 addition effects. La_2O_3 (Sigma Aldrich L4000) with a purity of more than 99.9 % and particle size of less than 20 μm was added in 1, 2, 3, and 4 wt.% to the base powder mixture. Micrographs of used powders are shown

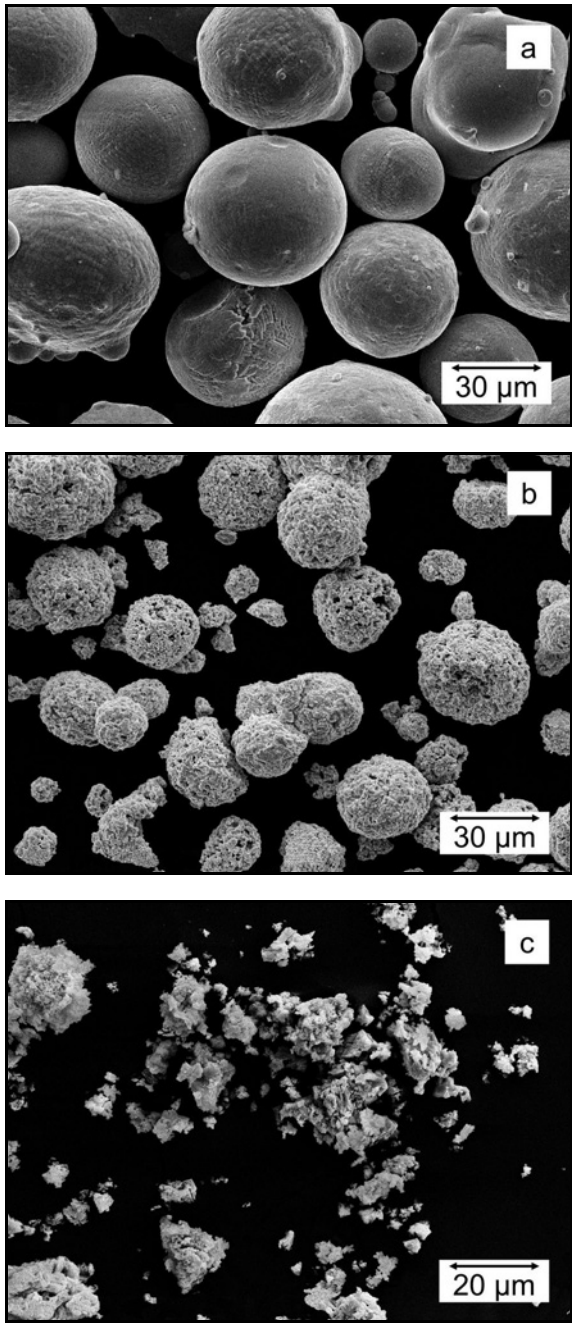

Fig. 1. SEM images of powders used for laser cladding of coatings: (a) NiCoCrAl, (b) WC, and (c) La_2O_3.

Table 2. Chemical composition of H13 hot work tool steel (wt.%)

	Fe	C	Si	Mn	Cr	Mo	V
H13	Bal.	0.36	0.97	0.23	5.41	1.6	1.17

in Figs. 1a–c. The prepared powder was mixed in a Turbula® mixer (Naraya-LTM-2000) for a duration and speed of 30 min and 60 rpm, respectively. H13 hot work tool steel was chosen as the substrate with the chemical composition given in Table 2. The samples were cut into cube shapes with dimensions of $10 \times 10 \times 10\,mm^3$ and then polished. The coatings were laser cladded using a setup equipped with a powder feeder attached to a 400 W pulsed Nd: YAG laser system. The used laser spot diameter was fixed at 2 mm. Argon was used as the shielding and carrier gas with flow rates of 20 and $15\,L\,min^{-1}$, respectively. The Nd: YAG laser pulse duration was fixed at 3.5 ms, so 35 Hz pulse frequency was established. The cladding was performed, and the procedure parameters were set as laser power of 250 W, scanning speed of $4\,mm\,s^{-1}$, powder feeding rate of $300\,mg\,s^{-1}$, and an overlap ratio of 50 %. Ultimately, the laser cladded coatings were then machined to an overall thickness of 200 µm. Coating parameters were determined by trial and error. The thickness of the coatings was also determined using a scanning electron microscope (SEM).

To investigate the isothermal oxidation, an electrical furnace was used (Shimifan 4000 W). First, the specimens were put in the furnace, followed by heating to 700 (± 5) ℃ at a rate of $10\,℃\,min^{-1}$. Then they were taken out of the furnace at different times (10, 20, ..., and 100 h) intervals followed by weighing using an electronic balance with a precision of ± 0.1 mg. Finally, to determine the oxidation kinetics equation, the specimen (coating with 4 wt.% La_2O_3) was put in another electric furnace equipped with a built-in electronic balance and heated for 10 h in the air atmosphere, where the weight of the specimen was being recorded continually.

The characterization of the phase structure of oxidized samples was carried out by X-Ray Diffractometer PANalytical X'Pert PRO (Netherland-2009) with Cu-kα radiation. The measurements were performed with a step size of 0.02° 2θ and a step time of 1 s.

Further morphological studies were carried out using MIRA3-Tescan field emission scanning electron microscope (FEG-SEM) and Jeol JXA-840 electron probe micro-analyzer (EPMA) equipped with wavelength dispersive spectrometer (WDS).

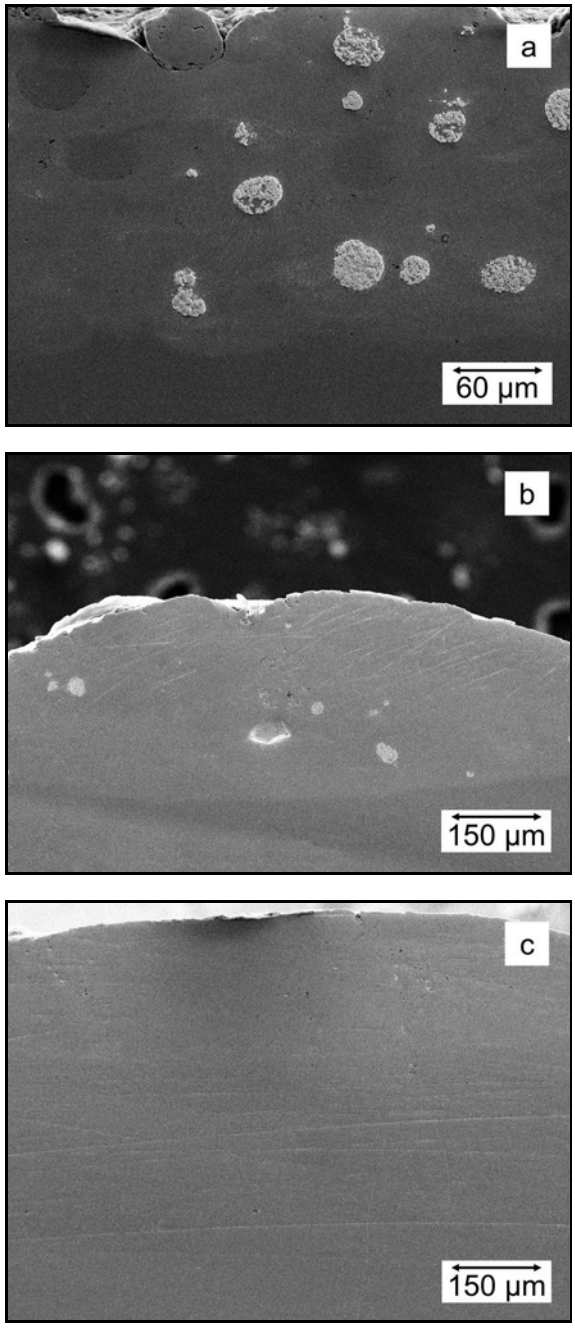

Fig. 2. SEM images of the cross-section of (a) NiCoCrAl – 30 wt.% WC – 2 wt.% La_2O_3, (b) NiCoCrAl – 30 wt.% WC, and (c) NiCoCrAl coatings.

3. Results and discussion

SEM images of the cross-section of the coating in Figs. 2a–c demonstrate the distribution of tungsten carbide and lanthanum oxide reinforcer seen as small

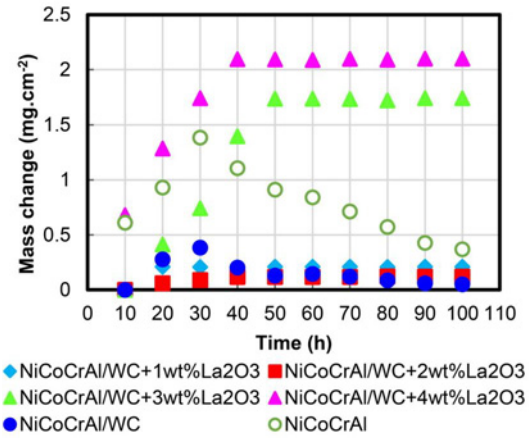

Fig. 3. Oxidation kinetics curves of the coatings.

white particles. The coatings have the least porosity and defects, which are the advantages of the laser cladding method.

3.1. *High-temperature oxidation behavior of coatings*

During heat treatment of the specimens, the isothermal oxidation of the coatings under a static air atmosphere changes the weight of the specimen at different time intervals. The recorded results are presented in a diagram in Fig. 3. As evident from the figure, the weight change of the coatings with La_2O_3 increases and stops after a while, then remains constant, indicating the end of the oxidation. The lowest weight increase is observed in coatings with 1 and 2 % La_2O_3, where the oxidation kinetics curves reached a plateau more quickly. Accordingly, it can be assumed that a compact and protective oxide layer is formed on the outer layer of the coating, slowing down or stopping the oxidation process. The figure also shows that the weight of coatings without La_2O_3 was increased up to 30 h of isothermal oxidation, and then it continually decreased. It is predicted that if the oxidation of La_2O_3 free coating continues for longer times, the weight changes will be negative, implying degradation of the coatings and even the substrate.

For detailed observation, the cross-section and surface of the specimens were examined by EPMA. Figures 4a–c show the EPMA images of the cross-section of the oxide layer formed on the coatings after oxidation at 700 °C for 100 h. As seen in Fig. 4a, a continuous oxide layer formed on NiCoCrAl/WC + 2 wt.% La_2O_3 coating. The coating and oxide layer thicknesses are about 200 and 20 µm, respectively. The oxide layer is compact and continuous, making interruption in connection between the coating and oxidizing environment. As a result, the cation diffusion into the interface of the oxide layer/oxidizing environment

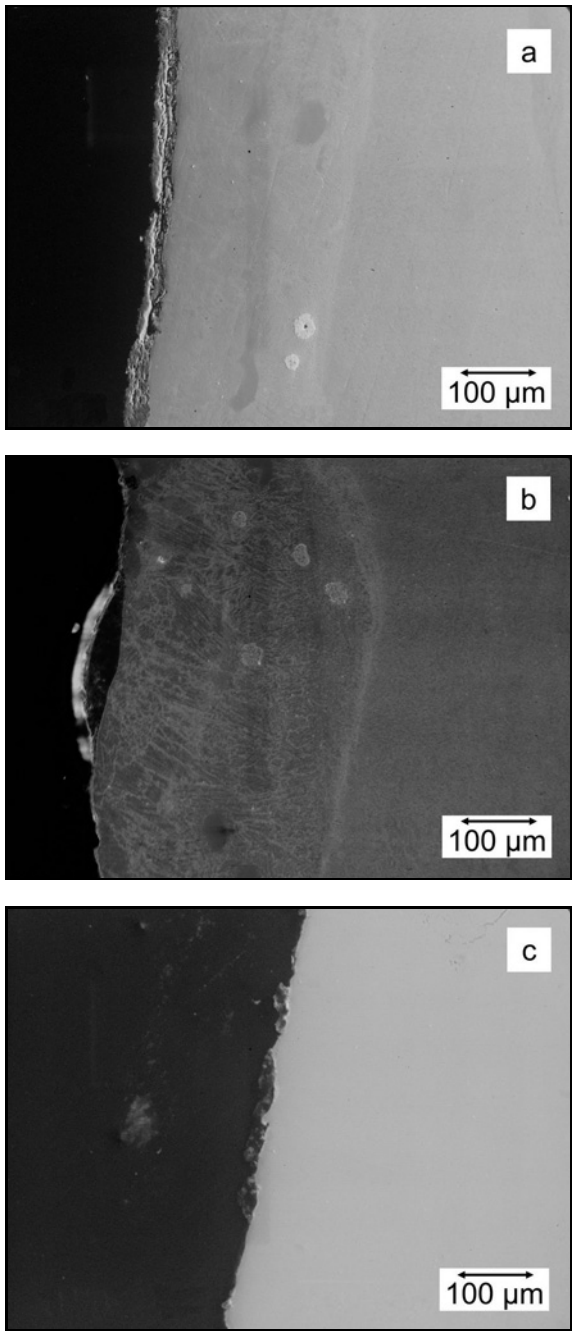

Fig. 4. Cross-section EPMA images of oxide layer of (a) NiCoCrAl/WC + 2 wt.% La_2O_3, (b) NiCoCrAl/WC, and (c) NiCoCrAl coatings oxidized at 700 °C for 100 h.

ought to be slowed down or stopped.

Consequently, the oxidation is slowed down or stopped, and the oxide layer acts as a barrier layer. The oxide layer formed on NiCoCrAl/WC coating indicated in Fig. 4b is torn and separated in some parts from the coating, causing the reconnection of the coating/oxidizing environment and continuing the oxidation process. This results in the gradual destruction of the coating. Figure 4c shows a flaked oxide layer

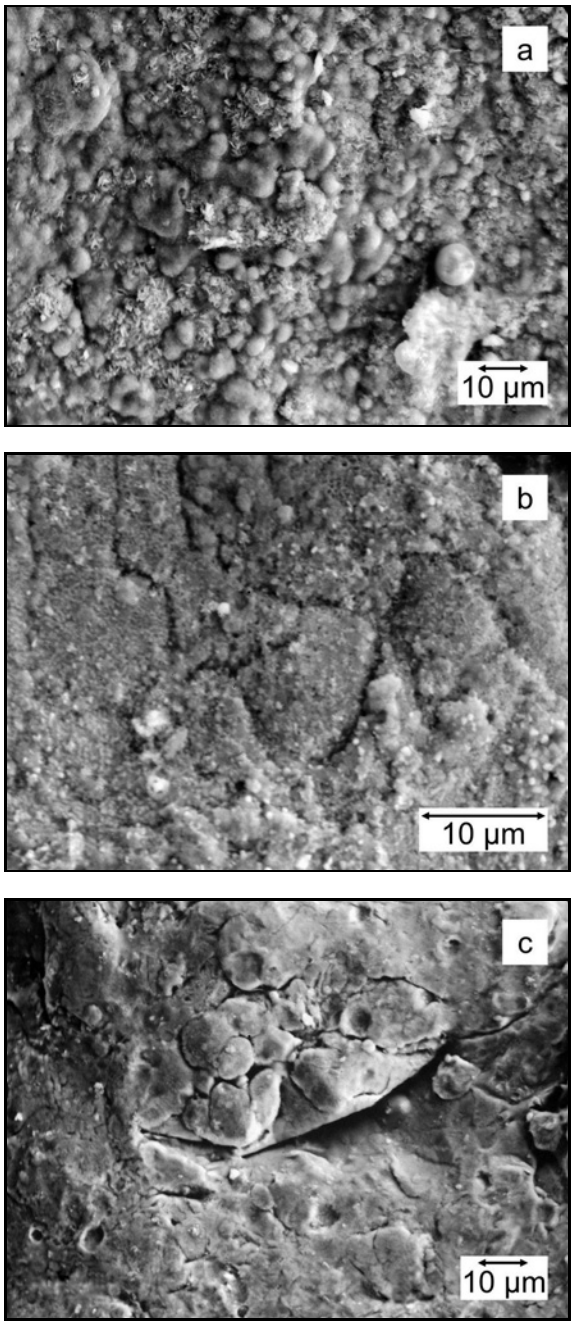

Fig. 5. EPMA images from the surface of oxide layers: (a) NiCoCrAl/WC + 2 wt.% La_2O_3, 20 h, (b) NiCoCrAl/WC, and (c) NiCoCrAl coatings, 30 h oxidation at 700 °C.

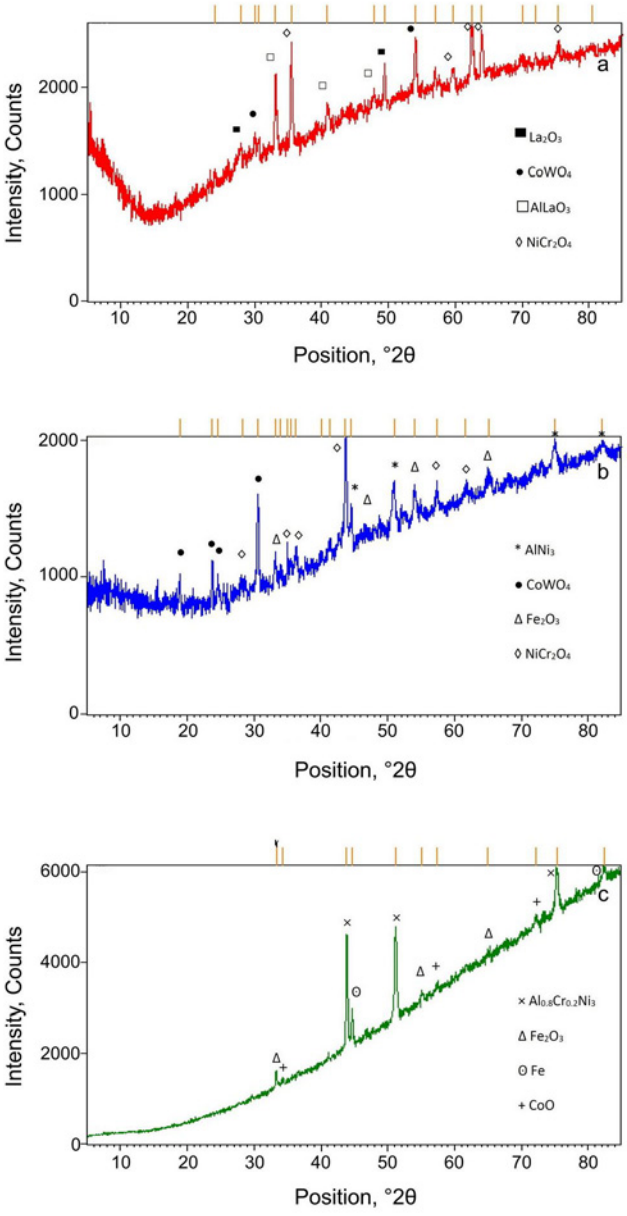

Fig. 6. XRD patterns of the surface of coatings after oxidation experiment at 700 °C: (a) NiCoCrAl/WC + 2 wt.% La_2O_3 for 100 h, (b) NiCoCrAl/WC for 50 h, and (c) NiCoCrAl for 100 h.

with an approximate thickness of 80 μm formed on NiCoCrAl coating where the coating degradation is observed.

Figures 5a–c show the EPMA images of the oxide layer surface which formed on the coatings after oxidation at 700 °C. Figure 5a displays a compact and crack-free oxide layer formed on the coating with 2 wt.% La_2O_3 after oxidation at 700 °C for 20 h. According to the image and diagram of Fig. 3, it can be presumed that the compact oxide film interrupts the connection between the coating/oxidizing environment resulting in the slow down or stop of the cation diffusion into the oxide. Figures 5b and 4c show the oxide layer formed on the La_2O_3 free coatings after 30 h of oxidation. The cracks can be observed in both figures, where they resulted in the detachment of the oxide layer in the continuation of the oxidation process. This eventually results in further contact of the oxidizing environment with the coating and further oxidation reactions. Detachment of the oxide layer can be demonstrated from

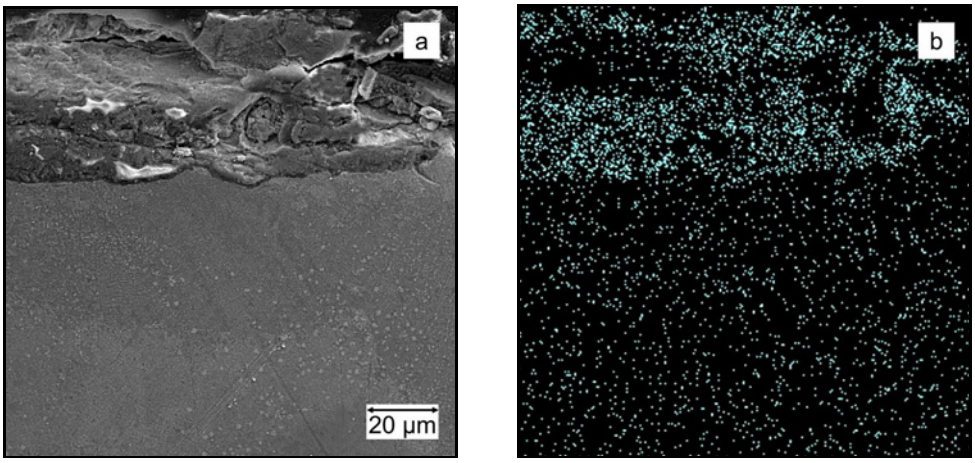

Fig. 7. (a) Cross-section FESEM images of oxide layer of NiCoCrAl/WC + 2 wt.% La_2O_3 coating after 100 h oxidation at 700 °C and (b) map of the distribution of oxygen in the oxide layer.

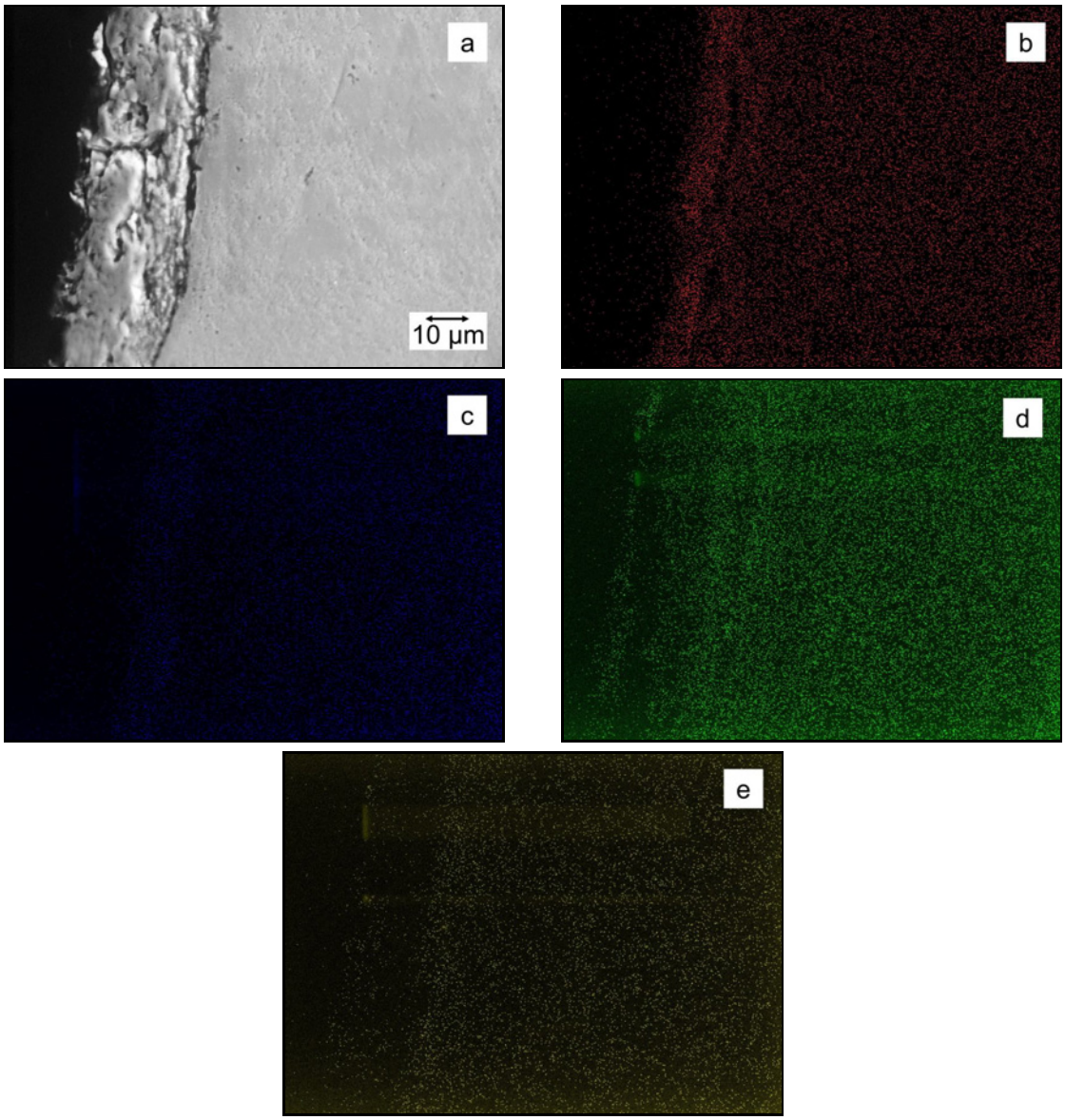

Fig. 8. (a) Cross-section EPMA images of the oxide layer of NiCoCrAl/WC + 2 wt.% La_2O_3 coating after 100 h oxidation at 700 °C and maps of the distribution of (b) Cr, (c) Ni, (d) Co, and (e) W in the oxide layer.

the diagram in Fig. 3 and the weight loss of the sample.

3.2. Mechanism of oxidation

The XRD patterns of the coatings after oxidation in air at 700 °C are shown in Figs. 6a–c. From the figure, it can be seen that in the pattern of La_2O_3 free coating, a peak belonging to Fe_2O_3 is detected, which has not appeared in the coating with La_2O_3. This could be due to the presence of La_2O_3 solid particles in the melt pool during laser cladding which by reducing the melt convection they reduced mixing of the melt sublayer and the coating. In Fig. 6a, it can be seen that $NiCr_2O_4$ spinel is present in the oxide layer formed on the coating with La_2O_3 and $NiCr_2O_4$ spinel and WO_3 oxide layer formed on the NiCoCrAl/WC coating. WO_3 has a high vapor pressure and evaporates at above 1300 °C, but it is stable at lower temperatures and forms as particles [23]. Therefore, $NiCr_2O_4$ spinel can boost the protective feature of the oxide layer.

Although Cr_2O_3 is a protective oxide, neither NiO nor CoO is protective. However, Cr_2O_3 is not adequately formed due to the low chrome concentration. But Cr_2O_3 with NiO can form $NiCr_2O_4$ spinel, where its distribution in the oxide film results in its compaction [23–25]. To characterize the coating, elemental mapping was carried out on the NiCoCrAl/WC + 2 wt.% La_2O_3 coating section. The oxygen map indicates that an oxide layer has been formed on the sample, Fig 7. EPMA mapping and WDS analysis were performed to investigate in detail the reason for the heterogeneous distribution of oxygen in the oxide layer and study the influence of coating elements to form oxide layers. Figure 8 shows the EPMA elemental maps of the oxide layer in NiCoCrAl/WC + 2 wt.% La_2O_3 coating. As shown in Fig. 8d, the nickel concentration is dramatically decreased in the coating at the oxide/coating interface. A high concentration of Cr is observed in the oxide layer adjacent to the oxide/gas interface, implying that short-path diffusion has been preferred due to the coating microstructure. The refinement of microstructure enhances short-path diffusion for the oxide formation as of Cr in this study. It increases the diffusion coefficient, accelerates selective oxidation, and ensures that the cladded coating possesses good oxidation resistance. Hence there might be an adequate opportunity for the formation of $NiCr_2O_4$ spinel and a compact-protective oxide layer. This compact layer slowdowns or stops the diffusion to the oxide layer, consequently slowing down or stopping the oxidation process [23–26].

Optical micrographs of the coatings are shown in Figs. 9a–c. The presence of La_2O_3 and its uniform distribution increased the heterogeneous nucleation sites in the melt pool and caused a fine equiaxed dendritic microstructure [15]. Although the microstructure of all

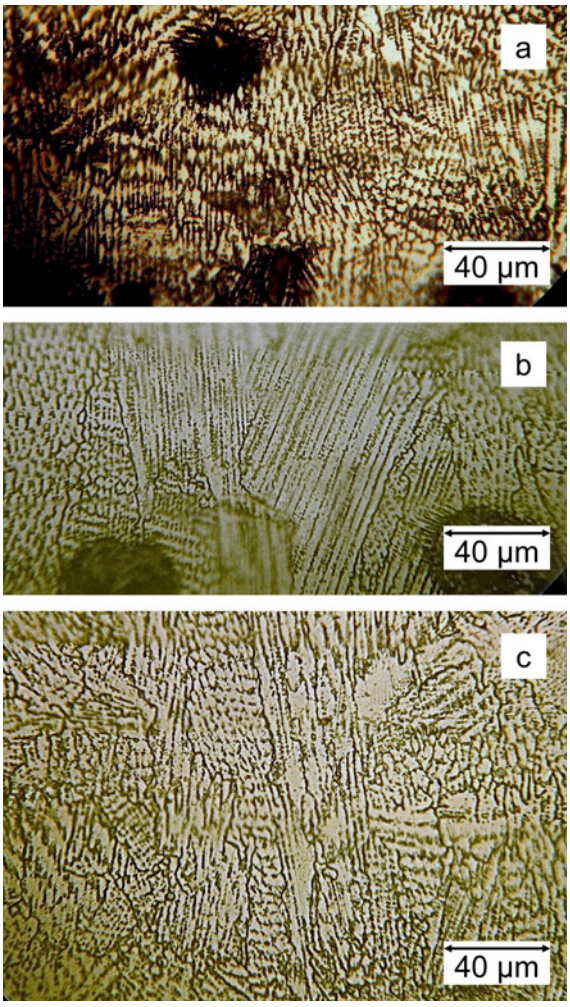

Fig. 9. Optical microscopy images of cross-section of coatings: (a) NiCoCrAl-30 wt.% WC – 2 wt.% La_2O_3, (b) NiCoCrAl-30 wt. % WC, and (c) NiCoCrAl.

the coatings should be fine-grained due to the rapid solidification in laser cladding, however, La_2O_3 presence results in the further refinement of dendrites and the equiaxed grain microstructure.

As discussed earlier, the images of Fig. 5 show that despite the formation of protective $NiCr_2O_4$ oxide on the NiCoCrAl/WC coating, it is not very stable where it cracks down and then collapses. To evaluate the reason, the WDS line-scan microanalysis results for five different lines from the coating toward the oxide layer of NiCoCrAl/WC + 2 wt.% La_2O_3 and NiCoCrAl/WC coatings are shown in Figs. 10a,b.

The free energy of chromium oxide formation is less than that of nickel and cobalt; however, the required activation energy for Cr^{3+} diffusion is equal to 61100 Cal mole^{-1} and is higher in comparison to Co^{2+} (34500 Cal mole^{-1}) and Ni^{2+} (45900 Cal mole^{-1}). Co^{2+} ions also have more mobility than other cations of the coating. Due to the high concentration of cobalt and nickel in the coating, diffusion of their

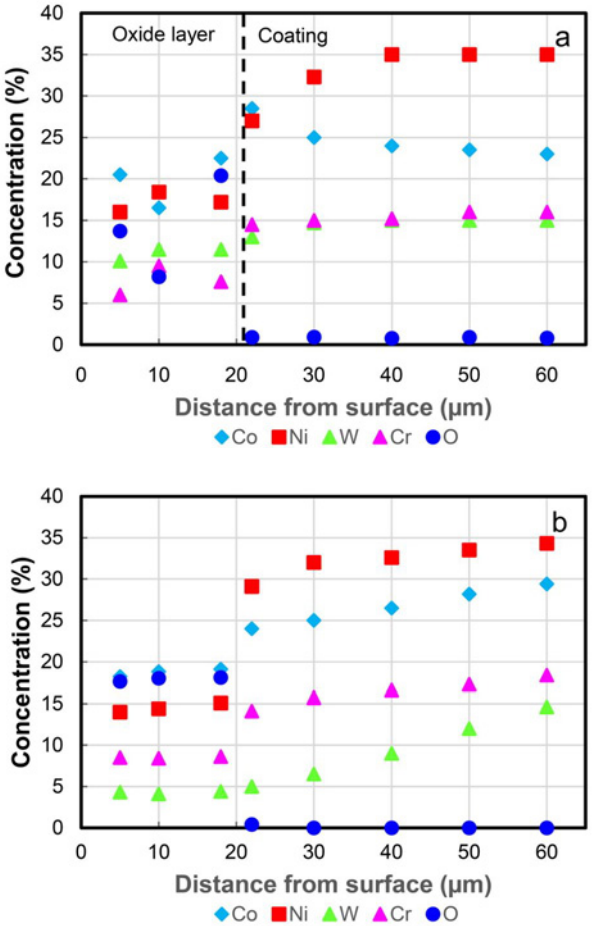

Fig. 10. The WDS line scan from the oxide scale to the (a) NiCoCrAl/WC + 2 wt.% La_2O_3 and (b) NiCoCrAl/WC coatings isothermally oxidized at 700 °C for 100 h.

cations is preferred to the other ones. According to the Ellingham-Richardson diagram, Gibbs free energy of the formation of cobalt oxide has a value less than that of nickel at 700 °C, then its formation is preferred. Moreover, due to selective oxidation, cobalt oxidation takes place more than other components in the coating. In Fig. 10a, it can be seen that the cobalt concentration is increased near the interface of the coating/oxide layer. This is indicative that cobalt with higher diffusion than the other cations has been aggregated at the interface. According to Figs. 8–10, it can be concluded that because of the ordered structure of coating with La_2O_3, the long path diffusion is delayed, and the oxide layer has adequate opportunity to slow down or stop the diffusion of cations by the formation of $NiCr_2O_4$ spinel through providing short-path diffusion for the elements [23, 27–29]. Although in NiCoCrAl/WC coating, Co^{2+} cation diffusion into the oxide layer is easily performed, the formation of CoO induces stress in the oxide layer. The cause of stress formation is that the specific volumes of the oxide and the metal consumed in its formation are rarely the same. The sign of the stress in the oxide may be related to the Pilling-Bedworth ratio (PBR):

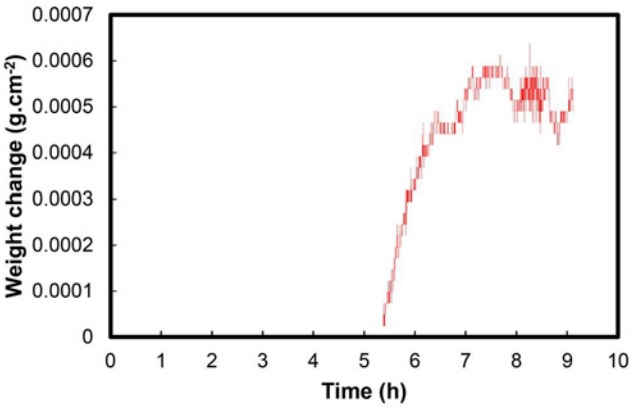

Fig. 11. Oxidation kinetics curve of the NiCoCrAl/WC + 4 wt.% La_2O_3 coating.

$$\mathrm{PBR} = V_{\mathrm{ox}}/V_{\mathrm{m}}, \tag{1}$$

where V_{ox} is the oxide volume and V_{m} is the metal volume. The ratio in Eq. (1) is 1.8 and 1.65 for cobalt and nickel, respectively, and 2.14 for Fe in Fe_2O_3 [30]. Subsequently, according to the Co and Fe penetration into the oxide layer in the La_2O_3 free coatings and consequently the formation of high volume oxides, the stress ought to be increased in the oxide layer and resulted in the formation of cracks and its collapse. Furthermore, the diffusion paths would be increased in the oxide layer, and the oxidation rate should be accelerated.

By increasing La_2O_3 in the coatings up to 4 wt.%, distortion in coatings structure and formation of energetic sites would occur. Hence, the energetic sites facilitate cation diffusion into the coating and make a delay for the oxide layer to be stable, resulting in the formation of a thicker oxide layer.

3.3. Oxidation kinetics equation

As shown in Fig. 3, none of the samples containing lanthanum oxide are oxidized in the first 10 h of the process except the sample containing 4 wt.% La_2O_3. The specimen coated with NiCoCrAl/WC + 4 wt.% La_2O_3 was put in an electric furnace at 700 °C, and the weight changes were recorded sequentially. The results are presented in Fig. 11. From the figure, it can be seen that no weight changes have been observed for the first 5 h of oxidation, implying that the coating oxidation has not occurred at this time. However, after 5 h, the weight changes are seen, meaning the onset of the oxidation process. By using the Python™ software and fitting a curve for the obtained data, the

parabolic equation for the oxidation process is determined as follows:

$$(\Delta m/A) = 0.4746 \times 10^{-3} t^2 - 0.8233 \times 10^{-3}, \quad (2)$$

where Δm is the weight change of specimen in g, A is the surface area of the oxidized specimen in cm^2, and t is the time in h. According to Eq. (2), the weight of the coating with 4 wt.% of La_2O_3 should be increased by 3.9 mg cm^{-2} after 100-hours oxidation at 700 ℃, however, as it can be seen from Fig. 3, the mentioned coating weight is increased by 2.1 mg cm^{-2} after more than 30 h oxidation at 700 ℃ and its oxidation process has been slowed down or stopped by the formation of a stable oxide layer.

4. Conclusions

Study of the isothermal oxidation kinetics of laser cladded NiCoCrAl/WC + La_2O_3 hybrid composite coatings leads to the following conclusions:

A stable and compact oxide layer has been formed by adding La_2O_3 to NiCoCrAl/WC coating, consequently decreasing and eventually stopping the specimen's weight changes. La_2O_3 particles acted as heterogeneous nucleation sites leading to the formation of a fine equiaxed dendritic microstructure. This has caused the possibility of forming a continuous and crack-free oxide layer and $NiCr_2O_4$ spinel through the short-path diffusion of the elements. $NiCr_2O_4$ spinel with its compact morphology could decrease or even stop the diffusion of cations and anions into the oxide layer, which ultimately pauses the oxidation process by preventing the connection between the coating and the oxidizing environments.

In the oxidation of NiCoCrAl/WC coating, the long-path diffusion provided the adequate concentration of Co and Fe ions during cladding where Fe entered the coating from the substrate. The selective oxidation of Fe and Co would be higher than other elements because of the high mobility of Co^{2+} and low Gibbs free energy of hematite. Also, concerning the high PBR ratio of both CoO and Fe_2O_3 oxides, the stresses induced in the oxide layer not only resulted in the formation of cracks in the coating but also caused the scaling of it and destroying the oxide layer leading to a weight decrease of the specimen. Even though $NiCr_2O_4$ spinel was formed in the prementioned coating oxidation, there was not enough time to form a protective layer. Hence, by establishing reconnection through the oxidizing agent environment and the coating, the oxidation would be continued. From the oxidation kinetics curve of the coating, it can be predicted that after about 100 h, the coating would be damaged, and the weight loss continues until specimen weight would be less than the initial weight.

The presence of La_2O_3 over 2 wt.% would cause distortion and highly-energetic sites within the coating. Thus the formation of a stable and compact oxide layer would be delayed due to the facilitation of the long-path diffusion. The outcome is the formation of a thicker oxide layer.

The oxidation kinetic curve of NiCoCrAl/WC + 4 wt.% La_2O_3 coating after oxidation in an electric furnace at 700 ℃ for 10 h was recorded by plotting the weight changes over time. A parabolic equation was derived for the oxidation kinetics using Python™ software. By comparing this equation and the results of the oxidation of the coating for 100 h, it could be realized that the coating resisted against oxidation with the formation of a sustainable and protective oxide layer after about 40 h.

Acknowledgement

The authors are acknowledging the Sahand University of Technology for providing the research facilities.

References

[1] Zhikun Weng, Aihua Wang, Xuhao Wu, Yuying Wang, Zhixiang Yang, Wear resistance of diode laser-clad Ni/WC composite coatings at different temperatures, Surf. Coat. Technol. 304 (2016) 283–292. doi:10.1016/j.surfcoat.2016.06.081

[2] Shi Hong Zhang, Ming Xi Li, Jae Hong Yoon, Tong Yul Cho, Characterization on the coatings of Ni-base alloy with nano- and micron-size Sm_2O_3 addition prepared by laser deposition, Mater. Chem. Phys. 112 (2008) 668–674. doi:10.1016/J.MATCHEMPHYS.2008.06.024

[3] Chun Guo, Jiansong Zhou, Jierong Zhao, Lingqian Wang, Youjun Yu, Jianmin Chen, Huidi Zhou, Microstructure and tribological properties of a HfB_2-containing Ni-based composite coating produced on a pure Ti substrate by laser cladding, Tribol. Lett. 44 (2011) 187–200. doi:10.1007/s11249-011-9837-z

[4] M. C. Sahour, A. Bahloul, A. B. Vannes, Characteristics of the laser clad metal made with powder mixture of Ni-based alloy and tungsten carbide, Int. J. Mater. Form. Suppl. 1 (2008) 1379–1382. doi:10.1007/s12289-008-0121-1

[5] G. Y. Liang, T. T. Wong, Investigation of microstructure of laser cladding Ni-WC layer on Al-Si alloy, JMEPEG 6 (1997) 41–45. doi:10.1007/s11665-997-0030-3

[6] J. Nurminen, J. Näkki, P. Vuoristo, Microstructure and properties of hard and wear resistant MMC coatings deposited by laser cladding, Int. J. Refract. Met. Hard Mater. 27 (2009) 472–478. doi:10.1016/j.ijrmhm.2008.10.008

[7] L. St-Georges, Development and characterization of composite Ni-Cr + WC laser cladding, Wear 263 (2007) 562–566. doi:10.1016%2Fj.wear.2007.02.023

[8] S. Nasiri Khalil Abad, J. Moghaddam, M. Mozammel, A. Mostafaei, M. Chmielus, Growth mechanism and charge transport properties of hybrid Au/ZnO nanoprisms, J. Alloys Compd. 777 (2019) 1386–1395. doi:10.1016/j.jallcom.2018.11.084

[9] Hongyu Wang, Dunwen Zuo, Xiangfeng Li, Kangmin Chen, Mingmin Huang, Effects of CeO_2 nanoparticles on microstructure and properties of laser cladded NiCoCrAlY coatings, Journal of Rare Earths 28 (2010) 246–250. doi:10.1016/S1002-0721(09)60089-2

[10] Shi Hong Zhang, Ming Xi Li, Tong Yul Cho, Jae Hong Yoon, Chan Gyu Lee, Yi Zhu He, Laser clad Ni-base alloy added nano- and micron-size CeO_2 composites, Optics & Laser Technology 40 (2008) 716–722. doi:10.1016/j.optlastec.2007.10.007

[11] N. Sobczak, R. M. Purgert, R. Asthana, J. J. Sobczak, M. Homa, R. Nowak, G. Bruzda, A. Siewiorek, Z. Pirowski, Wettability and reactivity of Y_2O_3 with liquid nickel and its alloys, Ceramic Engineering and Science Proceedings 36 (2016) 309–321. doi:10.1002/9781119211747.ch25

[12] Pei Quan Xu, Hong Ying Gong, Guo Xiang Xu, Jian Ping He, Zhi Shui Yu, Study on microstructure and properties of Ni-based alloy/Y_2O_3-deposited metals by laser cladding, J. Mater. Sci. 43 (2008) 1559–1567. doi:10.1007/s10853-007-2339-6

[13] Li Mingxi, He Yizhu, Yuan Xiaomin, Effect of nano-Y_2O_3 on microstructure of laser cladding cobalt-based alloy coatings, Appl. Surf. Sci. 252 (2006) 2882–2887. doi:10.1016%2Fj.apsusc.2005.04.038

[14] Da Shu, Xiangxiang Cui, Zhuguo Li, Jichao Sun, Jianbing Wang, Xu Chen, Sichao Dai, Wudong Si, Effect of the rare earth oxide CeO_2 on the microstructure and properties of the nano-WC-reinforced Ni-based composite coating, Metals 10 (2020) 383. doi:10.3390/met10030383

[15] Shi Hong Zhang, Ming Xi Li, Jae Hong Yoon, Tong Yul Cho, Characterization on the coatings of Ni-base alloy with nano- and micron-size Sm_2O_3 addition prepared by laser deposition, Mater. Chem. Phys. 112 (2008) 668–674. doi:10.1016/J.MATCHEMPHYS.2008.06.024

[16] Youjun Yu, Jiansong Zhou, Jiangmen Chen, Huidi Zhou, Chun Guoa, Lingqian Wanga, Lianbin Yang, Preparation, microstructure and tribological behavior of laser cladding NiAl intermetallic compound coatings, Wear (2012) 274–275. doi:10.1016%2Fj.wear.2011.09.011

[17] Shengfeng Zhou, Xiaoyan Zeng, Growth characteristics and mechanism of carbides precipitated in WC-Fe composite coatings by laser induction hybrid rapid cladding, J. Alloys Compd. 505 (2010) 685–691. doi:10.1016%2Fj.jallcom.2010.06.115

[18] E. Toyserkani, A. Khajepour, S. F. Corbin, Laser Cladding, CRS Press, 2004. ISBN 9780849321726

[19] M. Erfanmanesh, R. Shoja-Razavi, H. Abdollah-Pour, H. Mohammadian-Semnani, Influence of using electroless Ni-P coated WC-Co powder on laser cladding of stainless steel, Surf. Coat. Technol. 348 (2018) 41–54. doi:10.1016/j.surfcoat.2018.05.016

[20] M. Alizadeh, A. Cheshmpish, Electrodeposition of Ni-Mo/Al_2O_3 nano-composite coatings at various deposition current densities, Appl. Surf. Sci. 466 (2019) 433–440. doi:10.1016/j.apsusc.2018.10.073

[21] Z. Shafee, M. E. Bahrololoom, B. Hashemi, Electrodeposition of nanocrystalline Ni/Ni-Al_2O_3 nanocomposite modulated multilayer coatings, Mater. Des. 108 (2016) 19–26. doi:10.1016%2Fj.matdes.2016.06.018

[22] T. Shinde, Influence of carbide particle size on the wear performance of cryogenically treated H13 die steel, Surface Engineering 37 (2021) 1206-1214. doi:10.1080/02670844.2019.1701858

[23] M. Zarezadeh Mehrizi, M. Shamanian, A. Saidi, R. Shoja Razavi, Laser cladding of CoWSi/WSi_2 on Ni substrate and evaluation of its high temperature oxidation behavior, Ceram. Int. 40 (2014) 13447–13452. doi:10.1016%2Fj.ceramint.2014.05.065

[24] U. K. Chatterjee, S. K. Bose, S. K. Roy, Environmental Degradation of Metals, Marcel Dekker, New York, 2001.

[25] B. Song, K. T. Voisey, T. Hussain, High temperature chlorine-induced corrosion of Ni50Cr coating: HVOLF, HVOGF, cold spray and laser cladding, Surf. Coat. Technol. 337 (2018) 357–369. doi:10.1016/j.surfcoat.2018.01.025

[26] Hongyu Wang, Dunwen Zuo, Jing Yan Mingmin Huang, Xiangfeng Li, Effects of nanometer Al_2O_3 particles on oxidation behavior of laser cladding low Al NiCoCrAlY coatings, Oxid. Met. 74 (2010) 49–60. doi:10.1007/s11085-010-9197-3

[27] F. Omidbakhsh, A. R. Ebrahimi, S. H. Mousavi, R. A. Khosroshahi, S. Nazarpour, Effect of oxygen boost diffusion treatment on fatigue behavior of Ti-4Al-2V alloy, Surf. Coat. Technol. 205 (2011) 2954–2963. doi:10.1016/J.SURFCOAT.2010.11.004

[28] H. Ruiz-Luna, J. Porcayo-Calderon, J. M. Alvarado-Orozco, J. E. García-Herrera, L. Martinez-Gomez, L. G. Trápaga-Martínez, J. Muñoz-Saldaña, Electrochemical corrosion of HVOF-sprayed NiCoCrAlY coatings in CO_2-saturated brine, Journal of Thermal Spray Technology 25 (2016) 1330–1343. doi:10.1007/s11666-016-0449-x

[29] H. X. Zhang, D. Fruchart, E. K. Hill, L. Ortega, Z. K. Li, J. J. Zhang, J. Sun, L. Zhou, Crystal structure, corrosion kinetics of new zirconium alloys and residual stress analysis of oxide films, J. Nucl. Mater. 396 (2010) 65–70. doi:10.1016/j.jnucmat.2009.10.055

[30] N. Birks, G. H. Meier, F. S. Pettit, Introduction to the High-Temperature Oxidation of Metals, Cambridge University Press, 2nd Edition, 2006. doi:10.1017/CBO9781139163903